Materials Today Bio 30 (2025) 101426

Contents lists available at ScienceDirect

Materials Today Bio

journal homepage: www.journals.elsevier.com/materials-today-bio

Therapeutic effect of low-dose BMSCs-Loaded 3D microscaffold on early osteonecrosis of the femoral head

Minzheng Guo [a,b,1], Baochuang Qi [d,1], Zijie Pei [a,b,1], Haonan Ni [d], Junxiao Ren [d], Huan Luo [d], Hongxin Shi [d], Chen Meng [d], Yang Yu [a], Zhifang Tang [d], Yongqing Xu [d,**], Qingyun Xue [b,***], Chuan Li [c,d,*]

[a] Chinese Academy of Medical Sciences & Peking Union Medical College, PR China
[b] Department of Orthopedics, Beijing Hospital, National Center of Gerontology, Institute of Geriatric Medicine, Chinese Academy of Medical Sciences, PR China
[c] Kunming Institute of Zoology, Chinese Academy of Sciences, PR China
[d] Department of Orthopedics, 920th Hospital of Joint Logistics Support Force, PR China

ARTICLE INFO

Keywords:
Osteonecrosis of the femoral head
Stem cell
Microscaffold

ABSTRACT

The early treatment of Osteonecrosis of Femoral Head (ONFH) remains a clinical challenge. Conventional Bone Marrow Mesenchymal Stem Cell (BMSC) injection methods often result in unsatisfactory outcomes due to mechanical cell damage, low cell survival and retention rates, inadequate cell matrix accumulation, and poor intercellular interaction. In this study, we employed a novel cell carrier material termed "3D Microscaffold" to deliver BMSCs, addressing these issues and enhancing the therapeutic effects of cell therapy for ONFH. We injected 3D microscaffold loaded with low-dose BMSCs or free high-dose BMSCs into the femoral heads of ONFH rats and assessed therapeutic effects using imaging, serology, histology, and immunohistochemistry. To understand the mechanism of efficacy, we established a co-culture model of human osteoblasts and BMSCs, followed by cell proliferation and activity detection, flow cytometry analysis, Quantitative RT-PCR, and Western blotting. Additionally, RNA sequencing was performed on femoral head tissues. Results showed that the 3D microscaffold with low-dose BMSCs had a therapeutic effect comparable to high-dose free BMSCs. Osteoblasts in the 3D microscaffold group exhibited superior phenotypes compared to the non-3D microscaffold group. Furthermore, we have, for the first time, preliminarily validated that the low-dose BMSCs-loaded 3D microscaffolds may promote the repair of femoral head necrosis through the synergistic action of the MAPK and Hippo signaling pathways.

1. Introduction

ONFH (osteonecrosis of the femoral head) represents a prevalent and challenging orthopedic disorder. In its advanced stages, ONFH frequently precipitates femoral head collapse, concomitant with the onset of secondary osteoarthritis [1,2]. The pathogenesis of osteonecrosis of the ONFH remains a topic of ongoing debate and controversy. In addition to traumatic factors, common etiological factors encompass the misuse of glucocorticoids, alcohol abuse, coagulation dysfunction, sickle cell anemia, other hemoglobinopathies, inflammation, and autoimmune disorders. Among these, steroid-induced femoral head osteonecrosis prevails as the most frequently observed condition [3]. The current diagnosis and treatment of ONFH primarily rely on the ARCO staging system and individual patient factors. For patients in stage I and II according to the ARCO classification, conservation treatments such as immobilization, appropriate traction, medication, core decompression, osteotomy, and vascularized or non-vascularized bone grafting are commonly employed. The primary objectives are to alleviate pain and slow down the progression of necrosis. On the other hand, for patients in stage III and IV, total hip arthroplasty (THA) is often required. THA involves the complete replacement of the hip joint [4–6]. However, none of these methods have demonstrated the ability to reverse and cure early-stage ONFH. Furthermore, each method has its own limitations. For instance, while immobilization and traction, as well as medication,

* Corresponding author. Kunming Institute of Zoology, Chinese Academy of Sciences, PR China.
** Corresponding author.
*** Corresponding author.
[1] These authors contributed equally to this work and should be considered co-first authors.

https://doi.org/10.1016/j.mtbio.2024.101426
Received 22 October 2024; Received in revised form 14 December 2024; Accepted 23 December 2024
Available online 24 December 2024

carry a low risk of harm to patients, there is still debate regarding their effectiveness in alleviating long-term pain and slowing disease progression [7]. Various hip preservation surgeries may require patients to remain bedridden for an extended period after the procedure. Additionally, the low success rates and significant harm to patients associated with these surgeries have remained persistent concerns for many clinicians in the field. THA is the ultimate treatment option for patients with ONFH [8]. However, the lifespan of the artificial joint used in the replacement procedure is often limited. Additionally, the onset of ONFH has been occurring at a younger age in recent years. Consequently, an increasing number of scholars have turned their attention to early-stage treatments for ONFH, such as tissue engineering and regenerative medicine. This approach, which aims to facilitate self-repair of tissues and reverse early-stage osteonecrosis, has become a hot topic in current research [9,10].

Bone marrow mesenchymal stem cells (BMSCs) therapy, as a regenerative approach, has been increasingly utilized in research for treating early-stage ONFH. These cells possess the potential for self-renewal, multi-lineage differentiation, and immunomodulation. Furthermore, BMSCs exhibit excellent proliferative capacity, preserving their chromosomal karyotype and telomerase activity even after multiple passages [11–13]. The treatment of ONFH with BMSCs typically involves intra-bone marrow core decompression injection. However, this simple approach of solely injecting BMSCs often falls short of expected outcomes. Several factors may contribute to the suboptimal effects of direct BMSCs injection therapy, including mechanical damage to cells during the injection process, extensive infiltration of cells into surrounding tissue gaps leading to low cell retention rate, and compromised cell functionality due to inadequate extracellular matrix accumulation after injection. Therefore, a straightforward method to enhance the effectiveness of cell injection therapy is through high-dose multiple injections. This strategy, theoretically, can address the issues of low cell retention and survival rates [11,14]. However, the use of high-dose multiple cell injections increases treatment costs and reduces the practicality of cell therapy [15]. Furthermore, high-dose cell injections may lead to excessive cell expansion and uncontrollable aberrant mutations, particularly when using genetically modified cells, thereby further increasing the associated risks [14,16]. Therefore, the exploration of an efficient and safe cell therapy has become a current research hotspot, with suitable cell carrier materials emerging as a promising choice. The objective is to achieve cell protection and minimize cell damage during the injection process, while increasing cell retention and survival rates, ultimately improving the efficacy of cell therapy [17,18]. Common cell carrier materials are often in the form of hydrogels. However, hydrogels alone are not effective in promoting extracellular matrix accumulation or facilitating interactions between cells [16]. Therefore, we believe that ideal cell carrier materials should possess the following characteristics: 1) safety and non-toxicity with good cell compatibility; 2) injectability and biodegradability; 3) certain adsorption capacity to increase cell retention; 4) provide physical protection for cells; 5) create a physiologically relevant environment, such as a three-dimensional growth environment, to enhance the accumulation of extracellular mechanisms and interactions between cells. Ultimately, these properties improve cell utilization and prevent the need for high-dose repeated injections [19–22].

Therefore, our team has developed a 3D microscaffold material as a cell carrier. This microscaffold is stored in the form of tablets, which rapidly disperse into numerous microscaffold particles when dissolved in a neutral solution. Under a microscope, these microscaffold particles exhibit a three-dimensional structure with interconnected pores, providing a suitable environment for cell attachment and growth [23–25], while facilitating efficient transport of nutrients, oxygen and waste products. Instead of only increasing the surface area, as for traditional porous microspheres, our microscaffolds provide a 3D microenvironment that enables automatic and homogeneous loading of cells, matrices, and/or bioactive factors to construct tailored cellular niches. Our previous research has demonstrated that the microscaffold particles loaded with stem cells can enhance the therapeutic efficacy of cells. In a study using a rat model of knee osteoarthritis, we found that intra-articular injection of microscaffold-loaded low-dose stem cells produced similar therapeutic effects to the injection of high-dose stem cells alone [16,23].

In this study, we for the first time utilized a 3D microscaffolds loaded with low-dose bone marrow mesenchymal stem cells for the treatment of steroid-induced femoral head necrosis in a rat model. We also established an *in vitro* co-culture system of osteoblasts, MPS-induced osteoblasts, pure BMSCs, and BMSCs grown in 3D microscaffolds for the analysis and identification of osteoblasts within the co-culture system. And through RNA-seq analysis and molecular biology validation, we have, for the first time, preliminarily explored the mechanisms underlying the therapeutic effects of the low-dose BMSCs-loaded 3D microscaffolds in femoral head necrosis. These findings confirm that the 3D microscaffolds loaded with low-dose bone marrow mesenchymal stem cells may be a promising therapeutic strategy for early-stage steroid-induced femoral head necrosis.

2. Materials and methods

2.1. Experimental design

Human BMSCs were seeded in spinner culture flasks and co-cultured with 3D microscaffolds for 4 days, resulting in the formation of a microscaffold suspension loaded with BMSCs. Subsequently, these suspensions were injected into the rat femoral head necrotic area. A co-culture system was employed to investigate the effects of 3D microscaffolds loaded with human BMSCs and free human BMSCs separately on human osteoblasts under both steroid-induced and non-steroid-induced conditions. The flowchart of experimental design is shown in Fig. 1.

2.2. Isolation and cultivation of BMSCs from SD rats

Isolation and cultivation of bone marrow mesenchymal stem cells from SPF-grade SD rats weighing 100–150g: The rats were anesthetized, and their bones were aseptically isolated and rinsed with sterile phosphate-buffered saline (PBS). The ends of the bones were cut using ophthalmic scissors to expose the bone marrow cavity. The bones were then placed in a sterile culture dish containing 10 ml of fresh DMEM complete medium supplemented with 10 % fetal bovine serum. A 1 ml syringe was used to flush the bone marrow cavity with complete medium, collecting the flush solution in another culture dish. This flushing step was repeated until the flush solution became clear. The bone marrow suspension was then centrifuged at 1000 r/min for 5 min at room temperature to remove the supernatant. The cell pellet was resuspended in 6 ml of complete medium to create a single-cell suspension, which was transferred to a 25 cm2 culture flask in a humidified incubator. After 24 h of culture, the medium was changed to remove floating blood cells. Subsequently, the medium was changed every two to three days until cell proliferation reached confluence [26,27].

2.3. Morphological observation of 3D microscaffolds

The 3D microscaffolds, provided by School of Medicine, Tsinghua University, were stored in tablet form (Fig. 2A) [28]. One tablet of 3D microscaffolds was dissolved in phosphate-buffered saline (PBS), and after complete dissolution and dispersion, the mixture was centrifuged to remove the supernatant. The 3D microscaffolds were then sputter-coated with gold for 90 s and imaged using scanning electron microscopy (SEM; HITACHI, Japan).

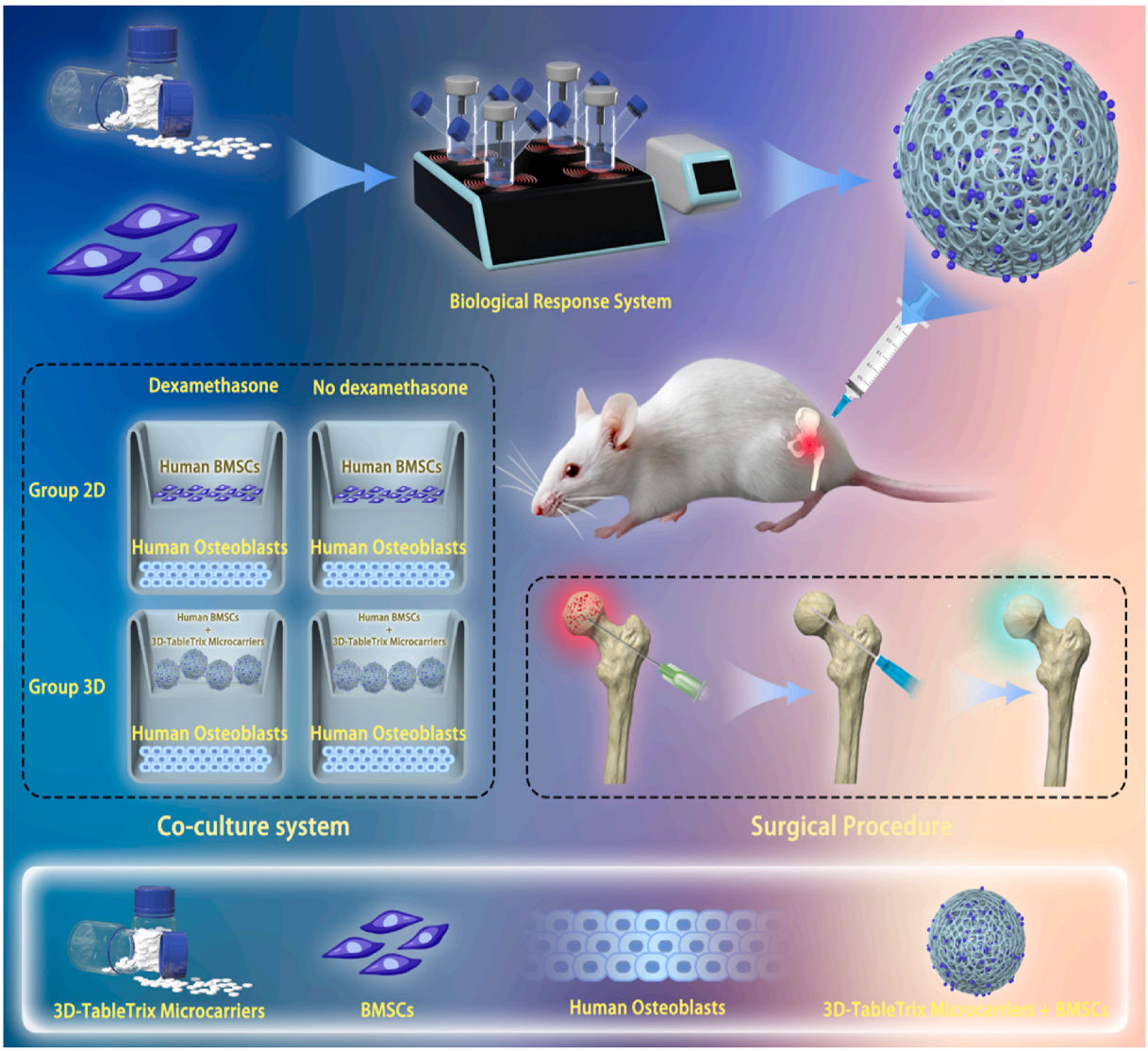

Fig. 1. The flowchart of experimental design.

2.4. Preparation and characterization of BMSCs-laden 3D microscaffolds

2.4.1. Preparation of BMSCs-laden 3D microscaffolds using the spinner culture flasks

Five 3D microscaffolds (specifications: 20 mg per microscaffold) were placed into a sterile 125 ml spinner culture flasks. Then, 20 ml of specialized complete medium was added to the culture bottle to fully dissolve the microscaffolds. Next, 1 ml of rat BMSCs suspension containing 2.5×10^6 cells were slowly added along the side wall of the spinner culture flasks. After that, an additional 30 ml of specialized complete medium was added to the culture bottle. The initial cell culture system comprising 50 ml was placed on a magnetic stirrer in a cell culture incubator, with an interval start-up consisting of 35 rpm/min for 5 min followed by 0 rpm/min for 1 h for a total of 24 cycles. The cell culture incubator maintained an environment of 37 °C and 5 % CO_2. On the following day, the speed of the spinner culture flasks was adjusted to a constant speed of 40 rpm/min, and 25 ml of fresh complete medium was supplemented. The culturing process continued for 21 days, during which the medium was replaced based on the glucose concentration in the culture supernatant [23,25].

2.4.2. Observation of BMSCs viability in 3D microscaffolds (live/dead staining)

Viability staining of BMSCs in 3D microscaffolds in the culture system was performed on days 1, 3, 7, 14, and 21. According to the manufacturer's instructions, a 100 μL suspension of cells and microscaffolds was extracted from the culture system and added to a 96-well plate. The supernatant was aspirated and Calcein AM and Propidium iodide (PI) (Wako, Japan) were added. The plate was then placed in a light-protected environment at room temperature for 20 min. Subsequently, the supernatant was discarded, and one PBS wash was performed. Finally, the stained samples were observed using a fluorescence microscope [14,16].

2.4.3. Quantitative RT-PCR of BMSCs in 3D microscaffolds

Quantitative RT-PCR was carried out on BMSCs in 3D microscaffolds on days 1, 3, 7, and 14. For each sample, reverse transcription was performed using the ReverTra Ace Qrna RT Master Mix with gDNA Remover (TOYOBO). Quantitative RT-PCR (qRT-PCR) was performed using the CFX96 Real-Time Quantitative PCR System (Bio-Rad, USA).

The samples were denatured at 95 °C for 30 s and then subjected to 40 cycles of amplification: initial denaturation at 95 °C for 1 min, denaturation at 95 °C for 20 s, annealing at 55 °C for 20 s, and extension at 72 °C for 30 s. Subsequently, fluorescence signals were collected and

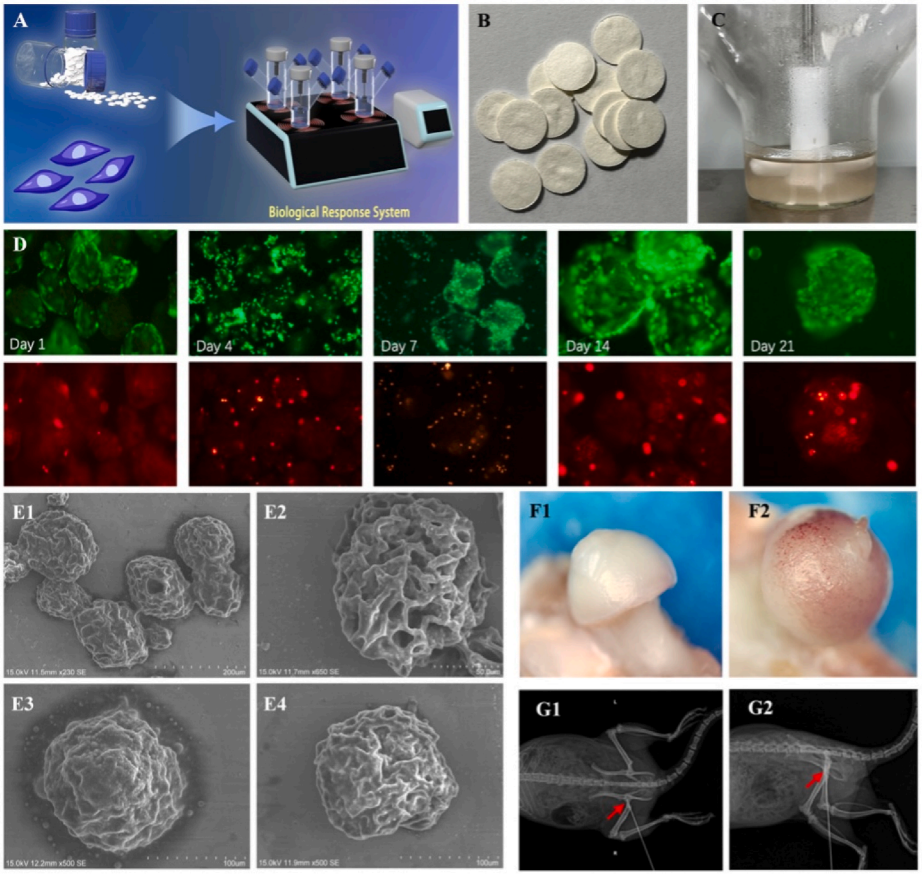

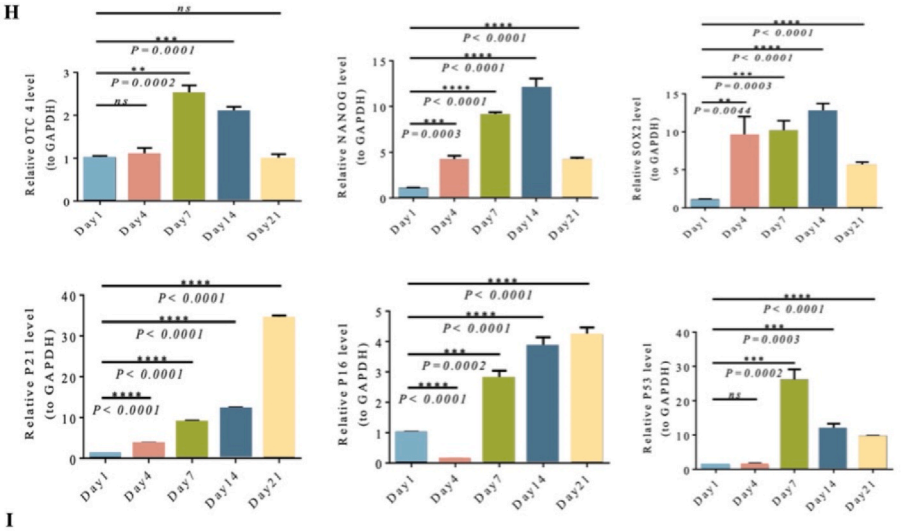

I

Surface Marker	Day 0	Day 3	Day 7	Day 14
CD73	99.2%	98.9%	95.8%	95.2%
CD90	99.8%	99.9%	99.9%	99.1%
CD105	96.4%	97.1%	98.2%	95.1%
CD34	0.2%	0.4%	1.9%	2.2%
CD45	0.5%	0.1%	1.5%	2.3%

(caption on next page)

Fig. 2. (A) 3D culture of BMSCs. **(B)** Packed 3D microscaffolds in a tablet form. **(C)** Morphology of 3D microscaffolds dispersed in culture medium. **(D)** Fluorescent images of live/dead staining of BMSCs on days 1, 4, 7,14 and 21 of culture. **(E1-E2)** Electron microscopy image of 3D microscaffolds. **(E3-E4)** BMSCs adherently grown on 3D microscaffolds. **(F1-F2)** Femoral head of SD rats. **(F1)** Normal femoral head. **(F2)** Femoral head after 8 weeks of MPS intervention. **(G1-G2)** Intraoperative X-ray image of a rat. **(G1)** Anteroposterior radiograph. **(G2)** Lateral radiograph. The red arrow: The insertion of a Kirschner wire into the necrotic area along the femoral neck. **(H)** Relative gene expression of stemness-related markers (SOX2, OCT4, NANOG) and senescence-related markers (P21, P16, P53) in BMSC-laden 3D microscaffolds over 21 days of culture (n = 3). **(I)** Flowcytometry analysis of surface biomarker expression over 14 days (n = 1, corresponding to a pool of 3 microscaffolds).

recorded to generate amplification curves and melt curves. Ct values were then determined. The Ct values of the products were normalized to glyceraldehyde-3-phosphate dehydrogenase (GAPDH) as an internal control, and the relative expression levels of the gene were calculated using the 2–ΔΔCT method.

2.4.4. Flow cytometry of BMSCs in 3D microscaffolds

SD rats' BMSCs were stained with antibodies against MSC markers CD73, CD90, and CD105, as well as negative markers CD34 and CD45. Unstained BMSCs were used as negative controls. The cells were analyzed by flow cytometry (BD LSRFortessa, US).

2.5. Co-culture model of human osteoblasts and human BMSCs in femoral head necrosis

2.5.1. Isolation and culture of human osteoblasts

Primary human osteoblasts were isolated from femoral heads of patients with steroid-induced femoral head necrosis requiring total hip arthroplasty (THA). All patients provided informed consent, and the study was approved by the Ethics Committee of the 920th Hospital of the Chinese People's Liberation Army Joint Logistic Support Force.

Inclusion criteria for patients were as follows: 1) End-stage primary steroid-induced femoral head necrosis. Exclusion criteria were: 1) Other types of femoral head necrosis. 2) Patients with underlying medical conditions that precluded surgery, such as diabetes, heart disease, etc.

The inclusion criteria for patient selection were: 1) End-stage primary steroid-induced femoral head necrosis. The exclusion criteria were: 1) Other types of femoral head necrosis, 2) Patients with underlying medical conditions that precluded surgery, such as diabetes, heart disease, etc. Femoral head specimens were obtained and carefully dissected to remove periosteum and soft tissues. The specimens were then trimmed into 1mm3 bone blocks and placed in culture dishes containing DMEM/F12 medium. The bone blocks were transferred to EP tubes containing 2–3 mL of PBS, vigorously shaken, allowed to settle for 30 s, and the supernatant was removed. This process was repeated 3 times using sterile PBS for rinsing. Subsequently, the bone blocks were treated with a red blood cell lysis buffer containing sodium bicarbonate (840 mg), ethylenediaminetetraacetic acid (EDTA, 37.2 mg), ammonium chloride (8.023 g), and double-distilled water (1000 ml) at a pH of 7.2 and a volume ratio of 1:3. The mixture was incubated for 8 min, centrifuged, and the supernatant was discarded. The bone blocks were placed in centrifuge tubes until they turned white. Then, a 10-fold volume of 2.5 g/L trypsin was added and pre-digested at 37 °C for 20 min in a constant temperature incubator. The digestion was terminated with fetal bovine serum, and the digestion solution was discarded. The bone blocks were washed twice with PBS. Subsequently, a 0.1 % solution of type I collagenase at a volume ratio of 1:8 was added, and the tubes were sealed and placed in a 37 °C water bath for 1 h of digestion with oscillation. After centrifugation at 1000 rpm for 5 min, the supernatant was discarded. The precipitation was washed with PBS and centrifuged again at 1000 rpm for 5 min. After removing the supernatant, the precipitation was resuspended in complete DMEM-F12 medium and pipetted to homogenize the cell suspension. The suspension was filtered through a sieve to remove non-osteoblastic cells and impurities, while retaining the bone particles. The remaining bone particles were subjected to three repeated digestions with type I collagenase. The cell suspension obtained from the three digestions was adjusted to a concentration of 5 × 105 cells/mL (as determined by trypan blue staining, with a cell viability of not less than 95 %) and seeded in sterile culture plates. The cells were cultured in a 37 °C, 5 % CO_2 incubator. 48 h after seeding, the medium was changed, and the suspended cells were discarded. The medium was changed every 2 days until the cells approached confluence, which was considered as passage 0 [29].

2.5.2. Co-culture of human osteoblast and human BMSCs using transwell

Primary isolated and identified human osteoblasts were cultured in α-MEM medium supplemented with 10 % fetal bovine serum and 1 % dual antibiotic (penicillin-streptomycin) and maintained at 37 °C with 5 % CO_2. When the cell confluence reached 70 %, the cells were treated with an equal volume of either 0 μmol/L or 1 μmol/L methylprednisolone (MPS) as an intervention. The cells treated with 0 μmol/L MPS served as the control group, while those treated with 1 μmol/L MPS represented the steroid-induced necrosis of the femoral head (SINFH) model group. After a 24-h intervention period, the osteoblasts were collected for co-culture. A transwell system was utilized to establish the co-culture system, which was divided into two groups: a 2D co-culture group and a 3D co-culture group. In the 2D co-culture group, the osteoblasts treated with 0 μmol/L intervention and the human osteoblasts treated with 1 μmol/L MPS were separately seeded at a density of 5×10^5 cells/mL in the lower chamber of the transwell co-culture system, while the same number of free human BMSCs (1×10^6 cells) was seeded in the upper chamber of the transwell system. In the 3D co-culture group, human osteoblasts were seeded in the lower chamber of the transwell system using the same method, and 3D microscaffolds loaded with human BMSCs (1×10^5 cells) were seeded in the upper chamber. In both co-culture groups, the two cell types were not completely physically separated but allowed interaction only through diffusion factors. The co-culture systems were incubated in a 5 % CO_2, 37 °C culture incubator for 48–72 h, and then the human osteoblasts were collected for subsequent analysis [30–32].

2.5.3. The CCK-8 assay

The osteoblasts from each co-culture group cultured for 48–72 h were collected for CCK-8 assay. CCK-8 reagent (10 μl per well) was added to the osteoblasts, and the culture plates were then incubated at 37 °C for 2 h inside the incubator. The optical density (OD) was measured at 450 nm.

2.5.4. EdU imaging detection

Osteoblasts from each co-culture group cultured for 48–72 h were collected for EdU proliferation staining. A 2X EdU working solution was prepared by diluting the final concentration of 10 μM EdU working solution with cell culture medium at a ratio of 1:500. Subsequently, 20 μM of preheated 2X EdU working solution was added to each well of a 6-well plate and the cells were incubated for an additional 2 h. After removing the fixative, cells were washed with 1 mL of wash buffer three times for 3–5 min each. The wash buffer was then removed, and 1 mL of permeabilization solution was added to each well, followed by incubation at room temperature for 10–15 min. After removing the permeabilization solution, cells were washed with 1 mL of wash buffer 1–2 times for 3–5 min each. Subsequently, 0.5 mL of Click reaction solution was added to each well and the culture plate was gently shaken to ensure even coverage of the reaction mixture on the samples. The plate was then incubated at room temperature in the dark for 30 min. Finally, images were captured, and the percentage of positive cells was calculated.

2.5.5. Alkaline phosphatase activity assay was performed on human osteoblasts

Alkaline phosphatase activity assay was performed on osteoblasts from each co-culture group cultured for 48–72 h. The collected osteoblasts were washed with PBS, fixed with ALP fixative for 3 min, and then rinsed with distilled water. Prepared ALP incubation solution (B1 and B2 diluted in a 1:1 ratio) was added dropwise to each group of osteoblasts. The samples were placed in a humid chamber and incubated in the dark for 15–20 min, followed by rinsing with distilled water. Subsequently, the samples were stained with nuclear Fast Red solution for 3–5 min, rinsed with PBS, and then examined under a microscope.

2.5.6. Flow cytometry analysis

Osteoblasts from each group were washed twice with PBS and adjusted to a cell density of 1×10^6 cells/ml. A 1 mL cell suspension was centrifuged at 1300 rpm for 5 min, and the supernatant was discarded. After resuspending the cells in 500 μL of buffer, staining was performed according to the standard protocol of the Anexin-V FITC/PI Cell Apoptosis Detection Kit. Stained samples were acquired using the BD FACSCalibur flow cytometer, collecting data from 10^5 cells per sample. Each sample was measured three times, and the results were obtained using FlowJo software. The proportions of viable cells, early apoptotic cells, late apoptotic cells, and dead cells were statistically analyzed.

2.5.7. Quantitative RT-PCR

Gene expression analysis of co-cultured osteoblasts in each group was conducted following the steps described in Section 2.2.3.

2.5.8. Western blotting

The expression levels of Wnt1 and β-catenin proteins in co-cultured osteoblasts from each group were assessed using Western blot analysis. Cytosolic proteins were extracted directly using radioimmunoprecipitation assay (RIPA) lysis buffer (Servicebio) supplemented with a cocktail of protease and phosphatase inhibitors. The protein concentration was determined using the BCA Protein Assay Kit (Beyotime Biotechnology). Western blot analysis was conducted utilizing a kit according to the manufacturer's instructions, and chemiluminescent signals were generated using ECL reagent (Affinity).

2.5.9. Immunofluorescence taining

Osteoblasts from each group were fixed in 4 % paraformaldehyde (PFA) for 15 min at room temperature, followed by permeabilization with 0.1 % Triton X-100 for 10 min. After blocking with 5 % bovine serum albumin (BSA) in phosphate-buffered saline (PBS) for 1 h at room temperature, the cells were incubated overnight at 4 °C with primary antibodies against osteocalcin (OCN) (Proteintech, America) and alkaline phosphatase (ALP) (ABclonal, America), each diluted at 1:200 (OCN) and 1:50 (ALP) in 1 % BSA/PBS. The following day, cells were washed three times with PBS and incubated with fluorescently labeled secondary antibodies (Donkey Anti-Mouse IgG H&L and Donkey Anti-Rabbit IgG H&L, Abcam, England) at a dilution of 1:400 for 1 h at room temperature in the dark. Nuclei were counterstained with 4′,6-diamidino-2-phenylindole (DAPI) (Abcam, England) for 5 min, followed by three washes with PBS. Fluorescent images were captured using a Zeiss LSM 710 confocal microscope under identical exposure settings. Quantification of fluorescence intensity was performed using ImageJ to ensure consistency across samples.

2.6. Animal experiments

2.6.1. Steroid-induced ONFH rat model

The animal experiments were conducted in accordance with the guidelines set by the Institutional Animal Care and Use Committees (IACUC), and approval was obtained from the Ethics Committee of the 920th Hospital of the People's Liberation Army Joint Logistic Support Force (Approval No. 2022-039-01). A total of 56 male Sprague Dawley rats (8–10 weeks old and weighing 250–300 g) were purchased from the Animal Experiment Center of Kunming Medical University. The subjects were randomly divided into the following groups: Control (n = 8), Low BMSCs/microscaffolds (n = 8) (1×10^5 cell), High BMSCs(n = 8) (1×10^6 cell), Low BMSCs (n = 8) (1×10^5 cell), microscaffolds (n = 8) (0.5–0.7 mg), Core Decompression (CD)(n = 8), ONFH(n = 8). Except for the control group and ONFH model group, the remaining rat groups were administered intramuscular injections of methylprednisolone (MPS) (Pfizer, America). The dosage was 60 mg/kg once daily for 7 consecutive days. Subsequently, all rats were carefully maintained for 8 weeks [33,34]. Surgical procedure: After preparing the surgical area and inducing anesthesia through inhalation, the rats were positioned in a lateral recumbent position. The surgical site was disinfected and covered with surgical drapes. The center of the femoral head was located, and a longitudinal incision was made along the axis of the femoral neck to expose the underlying tissues. Using a 0.8 mm Kirschner needle, a needle was inserted at a 19° angle, 20 mm from the knee joint, with a depth of approximately 5–6 mm. X-ray fluoroscopy was performed during the procedure to confirm successful placement of the puncture needle, as shown in Fig. 2(E1-E2). Subsequently, the tunnel was rinsed with saline solution to remove bone debris. Injection treatments were administered according to the design requirements of each group. Finally, the tunnel opening was sealed with bone wax, and the incision was meticulously closed layer by layer.

2.6.2. Micro-CT analysis

After 8 weeks of treatment, femoral heads were harvested and subjected to imaging scans using Micro-CT (SkyScan 1276, Germany, Bruker). The scanning parameters were set as follows: X-ray tube current of 200μA, voltage of 85 KV, scanning resolution of 10.141270 μm, exposure time of 384 ms, and a scanning angle of 180° [32]. The region of interest, which includes the subchondral bone 1 mm below the articular cartilage of the femoral head to the junction with the femoral neck, was scanned. Following the scan, the original images were reconstructed using three-dimensional reconstruction software NRecon (V1.7.4.2, Germany, Bruker), specifically selecting the region of interest. Subsequently, CT Analyser software (1.18.8.0, Germany, Bruker) was used to analyze the region of interest, including bone volume fraction (bone volume/total volume, BV/TV, %), trabecular spacing (Tb.Sp, mm), trabecular number (Tb.N, 1/mm), and trabecular thickness (Tb.Th, mm).

2.6.3. Histological and immunohistochemistry analysis

The femoral head tissues of each rat group were fixed in a 4 % paraformaldehyde solution for 48 h. After removal, they were washed three times with PBS for 20 min each time, followed by three washes with distilled water for 20 min each time. Subsequently, the femoral head tissues were decalcified in a 10 % EDTA decalcification solution for a duration of 6 weeks, with the decalcification solution being replaced every 7 days. After completion of decalcification, the specimens were consecutively dehydrated, embedded in paraffin, and sectioned into 4 μm paraffin slices. The prepared paraffin sections underwent the following tests: Hematoxylin-eosin (H&E) staining for histological observations of tissue morphology under a light microscope; Masson staining for evaluation of collagen fiber synthesis in the femoral head tissues of each group under a light microscope; immunohistochemical (IHC) staining with markers including OCN (Osteocalcin) and Ki67 to assess the metabolic state of the femoral head tissues; Terminal-deoxynucleotidyl Transferase Mediated Nick End Labeling (TUNEL) staining for observation of cellular apoptosis in the femoral head tissues of each group under a fluorescence microscope.

2.6.4. RNA-seq analysis of rats' femoral head

The total RNA in the femoral head tissues of three rat groups, namely the Control group (group Z), Low BMSCs/microscaffolds group (group A), and ONFH group (group L), was isolated and purified using TRIzol

reagent (Thermofisher, USA). Subsequently, the quantity and purity of the total RNA were assessed using a NanoDrop spectrophotometer (Nanodrop, USA), and the integrity of the RNA was evaluated using a bioanalyzer (Agilent, USA). The sequencing library was prepared using the NEBNext UltraTM RNA Library Prep Kit for Illumina (NEB, USA) following the manufacturer's instructions. The reference genome index was generated using Hisat2 v2.0.5. Differential expression analysis was conducted between groups (with two biological replicates per condition) using the DESeq2 R package. All statistical analyses were performed using the R statistical programming language. Genes with an adjusted p-value of <0.05 as determined by DESeq2 were considered differentially expressed. Differentially expressed genes (DEGs) were defined as those exhibiting a fold change ≥ 2 and a p-value ≤ 0.05. Heatmaps were created using the heatmap package. Gene ontology (GO) enrichment analysis and KEGG pathway analysis were carried out using the cluster Profiler R package. For each group, three replicates were collected for RNA-seq analysis.

2.7. Statistical analysis

Statistical analyses were performed using GraphPad Prism. All data are presented as mean ± standard deviation (SD). Student's t-test was used for comparing two groups, while one-way analysis of variance (ANOVA) followed by Tukey's post hoc test was used for comparing three or more groups. A value of $P < 0.05$ was considered statistically significant. All experiments were conducted using a minimum of three independent samples.

3. Results

3.1. Preparation and characterization of BMSCs-laden 3D microscaffolds

3.1.1. Morphological characteristics of 3D microscaffolds

The 3D culture of BMSCs is shown in Fig. 2A. The 3D microscaffolds are stored in the form of tablets and disperse into numerous individual microscaffolds particles when dissolved in neutral solutions such as physiological saline, culture media, or PBS (Fig. 2B and C). The scanning electron microscopy image is shown in Fig. 2(E1-E2). These microscaffolds particles exhibit a relatively uniform spherical or spheroid shape, with a diameter of 200 ± 7.35 μm. The microscaffolds particles are interconnected by numerous large pore structures, enabling cell adhesion and growth within these pore structures (Fig. 2(E3-E4)). Image analysis using ImageJ revealed an average pore diameter of 17.78 ± 6.3 μm in these microscaffolds particles.

3.1.2. Live/dead staining

Live/dead staining with Calcein AM/PI demonstrated abundant cell viability in the cells cultured in spinner culture flasks for 21 days, as shown in Fig. 2D. A comprehensive cell counts of 1.26×10^7 BMSCs was conducted on day 21 in the spinner culture flasks. To ensure both the quality and quantity of cells, we employed cells cultured in spinner culture flasks up to day 4 for animal experiments.

3.1.3. Quantitative RT-PCR of BMSCs in 3D microscaffolds

The BMSCs in 3D microscaffolds were evaluated for stemness and senescence related gene markers by qRT-PCR. The results indicated that the expression levels of stemness-related markers SOX2, OCT4, and NANOG were higher at day 4, day 7, and day 14 compared to other time points. In contrast, the senescence-related markers P21, P16, and P53 showed significant downregulation after 3 days, as shown in Fig. 2H. The collective gene expression results suggested that BMSCs maintained their stemness and suppressed senescence after being cultured in spinner flasks for 7–14 days. It is expected that similar effects will persist *in vivo* for at least 1–2 weeks after injection of 3D microscaffolds loaded with BMSCs pre-cultured until day 4.

3.1.4. Flow cytometry of BMSCs in 3D microscaffolds

Flow cytometry analysis indicated that during the 14 days 3D culture period, BMSCs within the 3D microscaffolds maintained their original immunophenotype, with high expression of BMSC markers CD73, CD90, and CD105, and low expression of negative markers CD34 and CD45, as shown in Fig. 2I. This demonstrates that the 3D microscaffolds do not alter the original immunophenotype of BMSCs, thereby providing evidence for the safety of cell culture using 3D microscaffolds to a certain extent.

3.2. Effects of 3D microscaffolds loaded with BMSCs on a steroid-induced femoral head necrosis model in SD rats

All rats survived for 8 weeks following intramuscular injection of MPS, and subsequent anatomical examinations revealed the presence of femoral head necrosis in all cases, as depicted in Fig. 2(F1) and **(F2)**.

3.2.1. μ-CT analyses

μ-CT analysis reveals alterations in trabecular bone architecture in the subchondral region of the femoral head in rats. As shown in Fig. 3A, the control group exhibited normal trabecular bone density, while the ONFH group displayed sparse trabecular arrangement and erosive changes in the medullary bone. The Low BMSCs/microscaffolds group and High BMSCs group exhibited denser trabecular arrangement compared to the control group. As shown in Fig. 3D-G, bone analysis software analysis demonstrated significantly increased BV/TV, Tb.N, and Tb.Th, as well as decreased Tb. Sp in the Low BMSCs/microscaffolds group and High BMSCs group when compared to the ONFH group, Low BMSCs group, microscaffolds group, and CD group. These findings suggest that 3D microscaffolds loaded with low-dose BMSCs effectively improve the reduced bone density induced by glucocorticoids and exhibit similar therapeutic effects to high-dose BMSCs administration.

3.2.2. Histological and immunohistochemistry analysis

Histopathological observations of femoral head necrosis using H&E staining. Results revealed that the control group exhibited normal histological features of femoral head tissue, with intact articular cartilage structure, regular cellular arrangement, absence of fissures, well-aligned trabecular pattern, uniform distribution of bone cells, and normal hematopoietic tissue distribution in the bone marrow cavity, without evident empty lacunae or increased adipocytes. In contrast, the ONFH group showed evident signs of femoral head necrosis, including reduced number of chondrocytes in the articular cartilage, nuclear shrinkage, decreased cell count, significantly thinner and even fractured trabeculae with sparse and reduced distribution, marked increase in red blood cell count, and noticeably elevated numbers of empty lacunae and adipocytes. Dense Trabecular Arrangement in the Low BMSCs/microscaffolds Group and High BMSCs Group compared to the ONFH Group, with reduced empty lacunae and adipocytes compared to the ONFH Group, as shown in Fig. 3B. The empty lacunae percentages for each group are presented in Fig. 3H. In conclusion, 3D microscaffolds loaded with low-dose BMSCs and high-dose BMSCs injection both exhibit similar effects on femoral head necrosis. Masson's staining results revealed minimal collagen fiber proliferation representing new bone tissue in the Control group. In comparison to the Control group, the ONFH group exhibited abundant red muscle fibers within the trabeculae, with no apparent increase in collagen fiber tissue. When comparing the Low BMSCs/microscaffolds group, High BMSCs group, ONFH group, and Control group, both the Low BMSCs/microscaffolds group and the High BMSCs group demonstrated significant collagen fiber proliferation, surpassing the other treatment groups, as shown in Fig. 3C and I. TUNEL staining was performed to observe cellular apoptosis in the rat femoral head tissue. The positive cells were labeled with red fluorescent staining on the sections. The overlay images of Tunel and DAPI staining revealed pink-colored positive cells. The apoptosis index was determined by randomly capturing 5 fields of view under high magnification on the

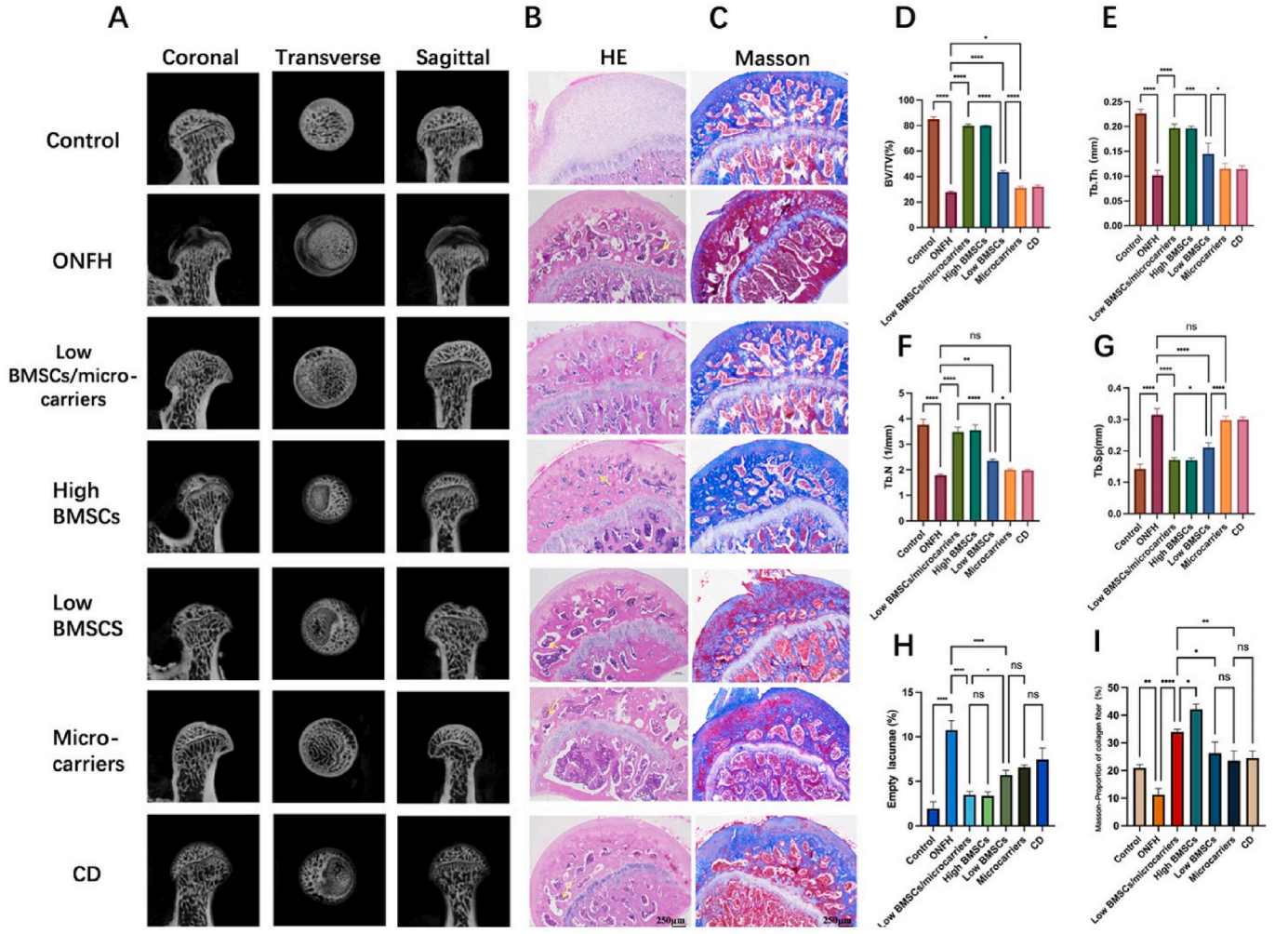

Fig. 3. (A) Images of μ-CT. **(B–C)** Histological (Hematoxylin & Eosin staining and Masson staining). The yellow arrow indicates increased adipocytes. **(D–G)** Quantitative analysis of BV/TV, Tb.N, Tb.Th and Tb. Sp in the femoral head. **(H)**The empty lacunae percentages of each group. **(I)** The collagen fiber proliferation.

same section and calculating the average ratio of positive cells in these 5 fields. Compared to the Control group, the ONFH group showed a significant increase in the apoptosis index ($p < 0.01$). In comparison, the Low BMSCs/microscaffolds group and the High BMSCs group exhibited a significant reduction in the apoptosis index ($p < 0.0001$), which was lower than other treatment groups. The results are shown in Fig. 4A and C. Immunohistochemical staining was conducted to evaluate the proliferation of osteoblasts in the rat femoral head tissue. Compared to the control group, the ONFH group exhibited a significant decrease in the expression level of osteocalcin (OCN) ($p < 0.001$). In comparison, both the Low BMSCs/microscaffolds group and the High BMSCs group demonstrated a significant increase in OCN-positive cells compared to the ONFH group ($p < 0.001$), surpassing other treatment groups. The findings are presented in Fig. 4B and D. Similarly, when compared to the Control group, the ONFH group displayed a significant decrease in the expression level of nuclear protein Ki67 ($p < 0.01$). In contrast, both the Low BMSCs/microscaffolds group and the High BMSCs group exhibited a significant increase in the percentage of Ki67-positive cells compared to the ONFH group ($p < 0.0001$), surpassing other treatment groups. The results are depicted in Fig. 4B and E.

3.3. *In vitro co-culture of human bone marrow mesenchymal stem cells and human osteoblasts*

Co-culture of human bone marrow mesenchymal stem cells and human osteoblasts was performed using Transwell inserts. Subsequently, the effects of 3D microscaffolds loaded with BMSCs and free BMSCs on human osteoblasts were evaluated through analysis.

3.3.1. *CCK-8 assay*

The CCK-8 assay results demonstrated that the osteoblasts in the 3D group exhibited significantly higher OD values compared to the 2D group, both in MPS-induced and non-induced environments (Fig. 5E), indicating statistically significant differences ($p < 0.0001$). This suggests that BMSCs cultured on 3D microscaffolds have a better ability to accumulate cell matrix, thereby promoting osteoblast vitality.

3.3.2. *EdU imaging assay*

The EdU imaging results revealed that the osteoblast positivity rate in the 3D group was significantly higher than that in the 2D group, both in MPS -induced and non-induced environments, with statistically significant differences (Fig. 5A and F). This indicates that BMSCs cultured on 3D microscaffolds have a greater ability to promote osteoblast proliferation.

3.3.3. *Alkaline phosphatase (ALP) assay*

The ALP detection results revealed a significantly higher percentage of ALP-positive osteoblasts in the 3D group, both in the presence and absence of MPS-induction, compared to the 2D group. These differences were statistically significant, as shown in Fig. 5B and G. This indicates that BMSCs cultured on 3D microscaffolds demonstrated enhanced expression of alkaline phosphatase by osteoblasts, thereby promoting

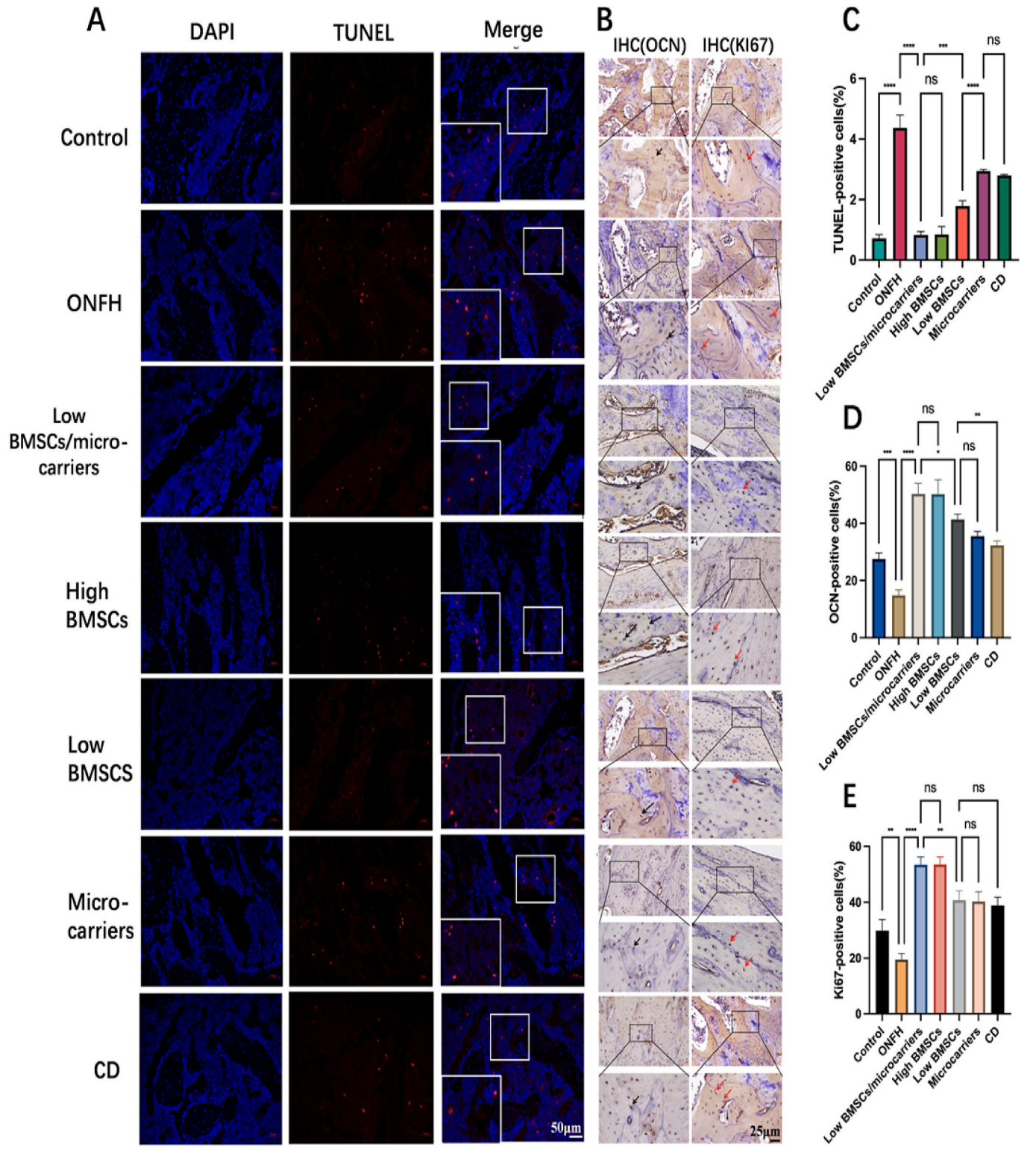

Fig. 4. (A) Tunel and DAPI staining. **(B)** Immunohistochemical staining (OCN and Ki67). The black arrow: OCN positive cells. The red arrow: Ki67 positive cells. **(C)** TUNEL positive cells percentages. **(D–E)** OCN positive cells percentages and Ki67 positive cells percentages of each group.

osteoblast activity more effectively.

3.3.4. *Flow cytometry analysis*

Flow cytometry analysis revealed significantly lower percentages of early apoptosis, late apoptosis, and dead cells in the 3D group of osteoblasts compared to the 2D group, both in the presence and absence of MPS-induction. These differences were statistically significant, as illustrated in Fig. 5C and H. These results suggest that BMSCs cultured on 3D microscaffolds exhibit enhanced maintenance of osteoblast activity, leading to reduced cellular apoptosis.

3.3.5. *Western blotting*

The Western blot analysis revealed significantly higher relative expression levels of Wnt1 and β-catenin proteins in the 3D group

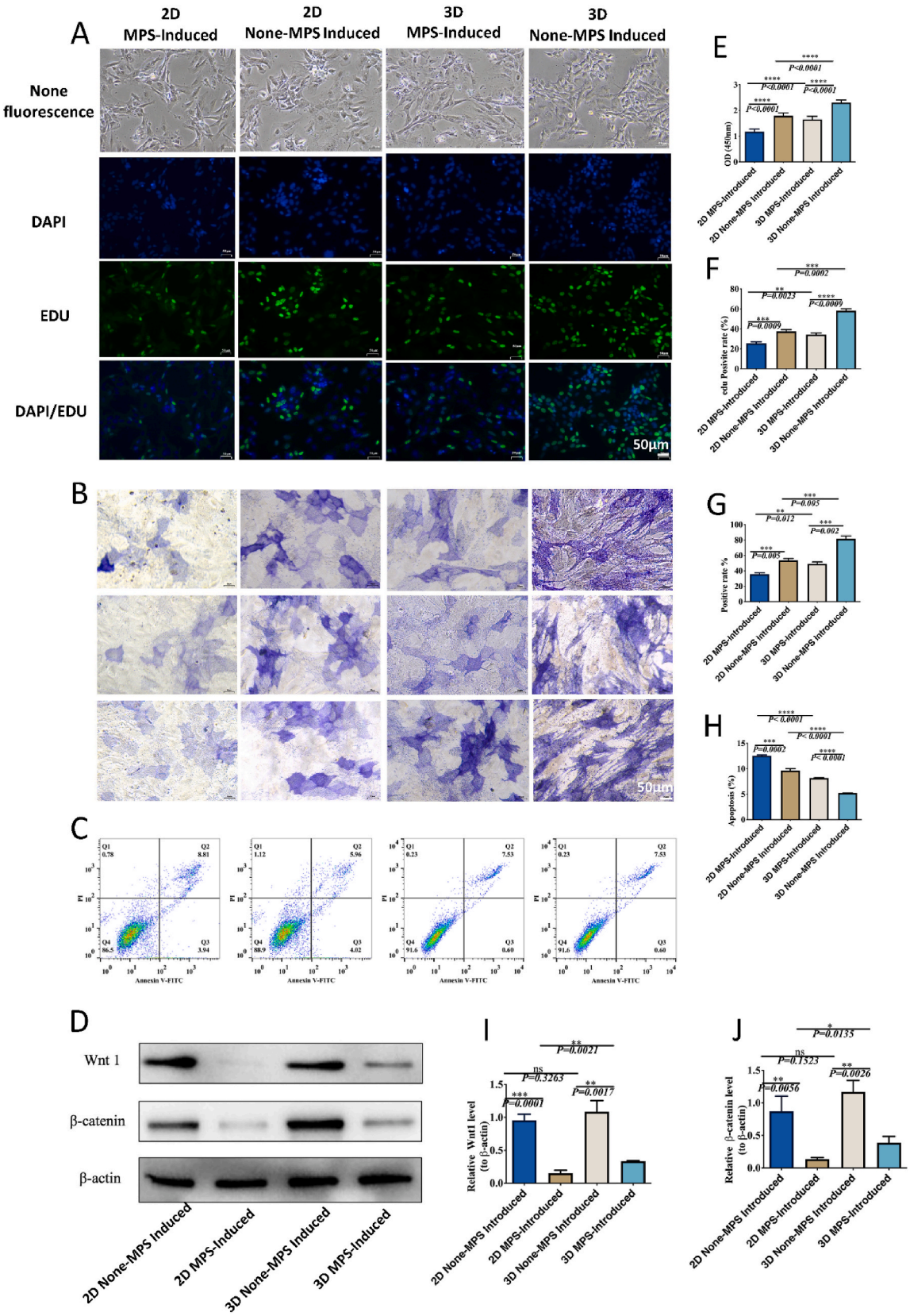

Fig. 5. (A) EdU staining of osteoblasts in 2D groups and 3D groups. **(B)** ALP staining of osteoblasts in 2D groups and 3D groups. **(C)** Apoptotic status of osteoblasts in different groups. Flow cytometry analysis results of osteoblasts. **(D)** Expression profile of Wnt1 and β-Catenin proteins. **(E)** CCK-8 assay. OD values of different groups. **(F)** EdU positive cell rates of different groups. **(G)** ALP positive cell rates of different groups. **(H)** Percentage of positive apoptotic cells in different groups of osteoblasts. **(I–J)** Grayscale intensity of Wnt1 and β-Catenin protein expression.

compared to the 2D group, both in the presence and absence of MPS-induction. These differences were statistically significant, as depicted in Fig. 5D, I and 5J. These findings indicate that BMSCs cultured on 3D microscaffolds can significantly activate the Wnt1/β-catenin pathway, promoting the relative expression levels of Wnt1 and β-catenin proteins, accelerating tissue repair in the necrotic area, and improving the condition of femoral head necrosis.

3.3.6. Immunofluorescence staining

Immunofluorescence staining demonstrated that the relative fluorescence density of OCN and ALP in the 3D group were significantly higher than those in the 2D group, irrespective of MPS induction (Fig. 6A). These differences were statistically significant, as shown in Fig. 6B and C. These findings indicate that culturing bone marrow mesenchymal stem cells on 3D microscaffolds enhances the expression of OCN and ALP in osteogenic cells, thereby promoting the repair of femoral head necrosis.

3.4. RNA-seq analysis of rats' femoral head

To gain insights into that early osteonecrosis of the femoral head was alleviated by cell therapy of low-dose BMSCs-loaded 3D microscaffold, the potential mechanisms were explored with bulk-RNA sequencing to identify the differentially expressed genes (DEGs) in the femoral head samples of each group. The samples were clearly separated into 3 expression patterns by a heatmap analysis of all identified expressed genes (Fig. 7A). Volcano plots showed 4379 DEGs between the group A and the group L, while 3807 DEGs were identified between the group L and the group Z (Fig. 7B).

KEGG (Kyoto Encyclopedia of Genes and Genomes) pathway enrichment analysis was conducted to assess the functions of these DEGs in biological functions. In comparison to the L group, several processes were found to be significantly upregulated in the A Group, Including MAPK signaling pathway, Hippo signaling pathway - multiple species, Calcium Signaling Pathway, Focal Adhesion, PI3K-Akt Signaling Pathway, Rap1 Signaling Pathway, Regulation of Actin Cytoskeleton and so on (Supplemental Table X1). In comparison to the Z group, several processes were found to be significantly down-regulated in the L Group, including ECM-Receptor Interaction, Hippo signaling pathway, MAPK signaling pathway, Rap1 Signaling Pathway, cGMP-PKG Signaling Pathway, Regulation of Actin Cytoskeleton, Cell Adhesion Molecules and so on (Supplemental Table X2). Furthermore, 15 key pathways related to the proliferation and osteogenic differentiation were selected (Supplemental Table X3) and analyzed for the regulation of gene expression, between and the A group and the L group, demonstrating that MAPK signaling pathway and Hippo signaling pathway were significantly up-regulated (Supplemental Table X4). The mitogen-activated protein kinase (MAPK) pathway, also known as the RAS-RAF-MEK-ERK pathway, is a critical intracellular signaling cascade that facilitates the repair of femoral head necrosis by promoting osteogenic differentiation, enhancing angiogenesis, suppressing apoptosis, and modulating inflammatory responses. Similarly, the Hippo signaling pathway contributes to the repair process by regulating mesenchymal stem cell (MSC) differentiation, promoting vascularization, and maintaining bone homeostasis, thereby providing essential cellular and vascular support (Fig. 7C–E).

KEGG pathway enrichment analysis indicating that TGFBR2, TGFB3, MPK2A6, P38, HSPB1, HSPBA1s genes were up-regulated in MAPK signaling pathway, focusing on TGFBR2, MPK2A6, HSPB1; FRMD6, YAP1, LTS1_2, TEAD, CCND1 genes were up-regulated in Hippo signaling pathway, focusing on YAP1, TEAD, CCND1 (Supplemental Table X5). Therefore, on the basis of the sequencing results, we speculate that MAPK signaling pathway and Hippo signaling pathway may be activated during the low-dose BMSCs-loaded 3D microscaffolds treatment of ONFH, these two pathways do not function in isolation; instead, they act synergistically to regulate key processes such as osteogenic differentiation, angiogenesis, and bone homeostasis, collectively driving the regeneration and repair of necrotic bone tissue. The rats' femoral head tissues were analyzed again to test this hypothesis. Western blot analysis revealed that the expression levels of TGFBR2, MPK2A6, and HSPB1 in the MAPK signaling pathway were significantly elevated in group A compared to group L (Fig. 7F). Similarly, in the Hippo signaling pathway, the expression levels of YAP1, TEAD, and CCND1 were significantly elevated in group A than in group L (Fig. 7G). The statistical analyses are presented in Fig. 7H and I.

4. Discussion

In this study, we utilized an SD rat MPS-induced femoral head necrosis model and an *in vitro* co-culture model to investigate the therapeutic effect of 3D microscaffolds loaded with BMSCs on MPS-induced femoral head necrosis. Clinical evidence currently suggests that repeated high-dose injections of stem cell therapy demonstrate better treatment outcomes compared to single injections, although they also carry higher risks of infection and other complications [35]. In animal experiments and *in vitro* co-culture studies, we have demonstrated, using methods such as Micro-CT, histology, and immunohistochemistry, that injection of 3D microscaffolds loaded with low-dose BMSCs exhibits similar therapeutic effects to high-dose BMSCs administered alone. Furthermore, through high-throughput sequencing of rat femoral head tissues, we have revealed the underlying molecular mechanisms of 3D microscaffolds loaded with low-dose BMSCs in the treatment of ONFH.

In recent years, regenerative medicine has rapidly advanced, and the integration of stem cells with biomaterials has emerged as a fundamental strategy for treating various diseases [36]. Mesenchymal stem cells (MSCs) from various tissue sources are considered reliable cell types for tissue repair due to their high proliferative capacity and multipotency [37,38]. Among them, bone marrow derived MSCs (BMSCs) have gained increasing attention in the field of orthopedics due to their low immunogenicity, ease of culture and expansion, and multilineage differentiation potential. While it is generally believed that stem cell therapy is dose-dependent and that a higher cell quantity leads to greater efficacy, further high-quality evidence is necessary to establish the long-term safety and clinical advantages of high-dose stem cell injections [39,40]. It is worth noting that stem cells frequently undergo excessive expansion in two-dimensional (2D) culture, leading to a loss of their stemness and phenotypic characteristics. Therefore, the use of 2D culture methods for cell mass production is not an ideal approach [41,42]. It is well known that 3D culture provides stem cells with the ability to establish biomimetic hierarchical structures, thereby better maintaining their activity [40,43]. However, a safe, stable, and efficient method for 3D culture of stem cells and achieving mass production has been a challenge. In this study, the novel cell carrier material, 3D microscaffolds, which we used, offers a potential cell delivery platform to address this challenge. Numerous studies have shown significant advantages of 3D microscaffolds compared to other existing cell carrier materials [24]. The microscaffolds used in this study are made from clinically applicable gelatin, which provides inherent cell adhesion motifs. Their 3D porous structure offers a natural growth microenvironment for BMSCs, thereby enhancing the retention rate and functionality of injected cells post-injection [16]. In this study, we employed 3D microscaffolds for the extended 14-day 3D cultivation of BMSCs. Subsequently, we substantiated the safety and efficacy of BMSCs loaded onto 3D microscaffolds through live/dead staining, quantitative RT-PCR, and flow cytometry analysis.

In our experimental study, we induced ONFH by intramuscular injection of glucocorticoids in rats. This model clearly establishes a relationship between glucocorticoids and the occurrence of ONFH [34]. At the 8th week after glucocorticoid injection, histological examination revealed ONFH in all rats. We conducted corresponding therapeutic interventions on the rats according to a pre-designed grouping. Through imaging, histology, and immunohistochemistry analysis, we found that,

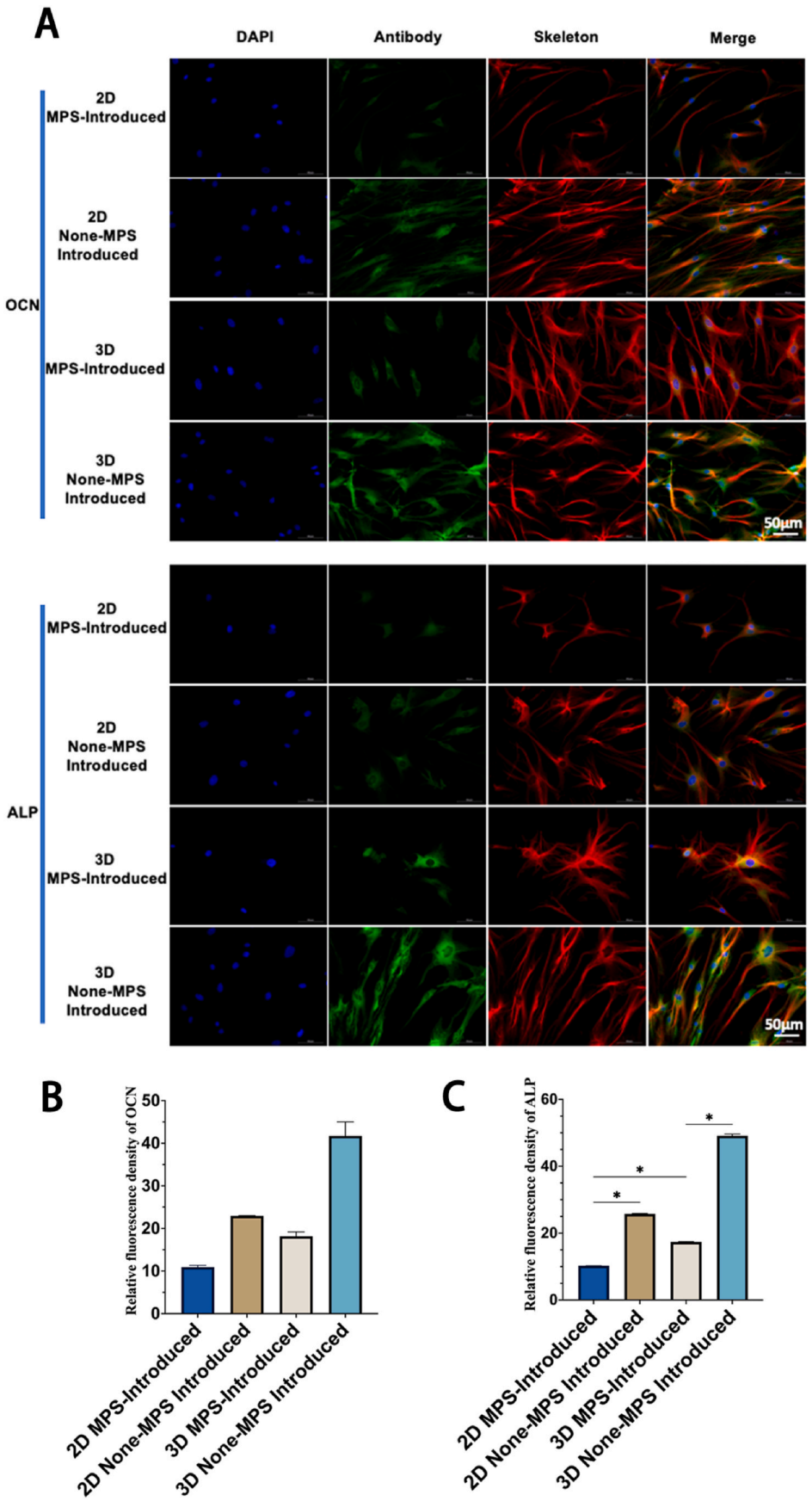

Fig. 6. (A) OCN and ALP immunofluorescence staining of each group. **(B–C)** Semi-quantitative analysis of OCN and ALP immunofluorescence intensity (n = 3). Statistical analysis was performed using an ANOVA with Tukey's post hoc test. Statistical significance was set at $P < 0.05$.

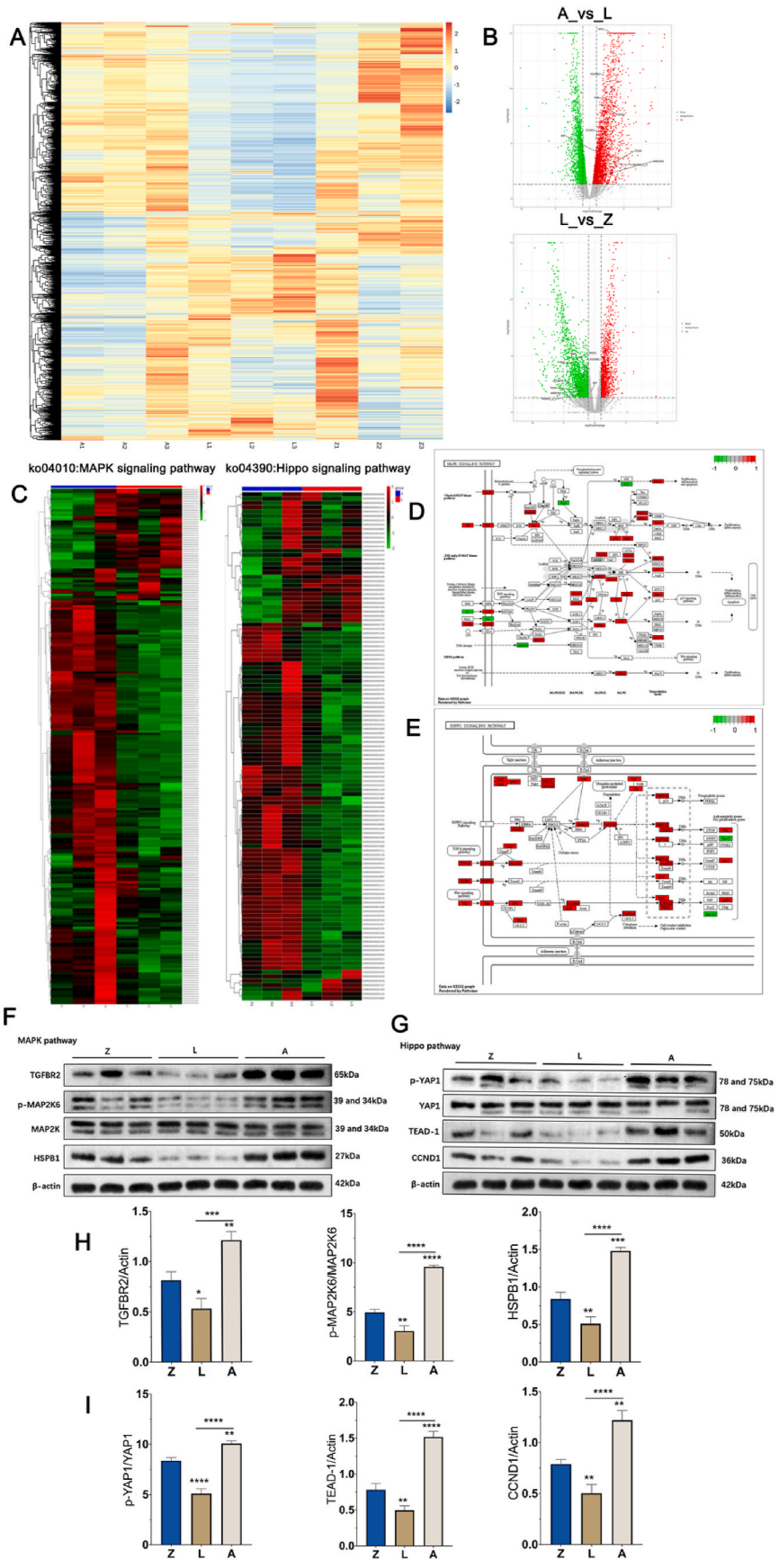

(caption on next page)

Fig. 7. (A) Differential gene clustering plot of Group Z, Group A and Group L. **(B)** Differential gene volcano plot of Group A vs Group L and Group L vs Group Z. **(C)** Heatmap of gene expression differences between group A and group L in the MAPK signaling pathway and Hippo signaling pathway. **(D)** Signal pathway diagram of MAPK signaling pathway. **(E)** Signal pathway diagram of Hippo signaling pathway. **(F)** Expression of TGFBR2, MPK2A6 and HSPBl protein in MAPK signaling pathway in each group of samples. **(G)** Expression of YAP1, TEAD and CCNDl protein in Hippo signaling pathway in each group of samples. **(H–I)** Statistical analysis of each protein expression (n = 3).

at 8 weeks post-intervention, the injection of 3D microscaffolds loaded with low-dose BMSCs showed similar therapeutic effects in repairing ONFH compared to the injection of high-dose BMSCs alone. Furthermore, both methods exhibited better therapeutic outcomes than the other treatment groups. Due to the limited source of primary BMSCs and the high cost of cell expansion culture, large-scale production of BMSCs for clinical application may not be economically or practically feasible. It is worth noting that stem cell injection therapy is more suitable for early-stage ONFH without obvious collapse, while its therapeutic efficacy is often poor for late-stage ONFH classified as Arco stages III and IV. In the early stages of ONFH, the synovial fluid can provide nourishment to the femoral head, and there may be inherent repair mechanisms. As a result, there are no apparent changes in articular cartilage. If early-stage ONFH is not promptly repaired, it will gradually progress into typical ischemic necrosis, where joint replacement surgery becomes the only effective treatment method [44].

Cell-cell interactions encompass a myriad of biological phenomena, including embryonic development, tissue morphogenesis, and repair [45,46]. Establishing a co-culture model of BMSCs and primary osteoblasts to simulate the physiological or pathological environment *in vivo* is an ideal research approach for investigating cell-cell interactions and evaluating therapeutic efficacy. In this model, BMSCs are surrounded by osteoblasts but do not directly contact them [32]. In this study, we established a co-culture model of human osteoblasts and human BMSCs using Transwell and analyzed the osteoblasts in the model. Flow cytometry analysis and protein expression results demonstrated that BMSCs grown in 3D microscaffolds, both in the physiological and pathological environments, could better enhance osteoblast activity and maintain their phenotype. These findings suggest that 3D microscaffolds loaded with BMSCs may potentially facilitate bone repair in femoral head osteonecrosis more effectively. As a cell delivery vehicle, if these BMSC-loaded microscaffolds are applied clinically, we speculate that BMSCs primarily exert their therapeutic effects on femoral head osteonecrosis repair through cell matrix accumulation and paracrine function. Additionally, the use of 3D microscaffolds may minimize mechanical damage to cells during the injection process, thereby improving the retention and viability of BMSCs *in vivo*.

Furthermore, this study has certain limitations. In our co-culture model of human BMSCs and human osteoblasts, we only investigated their phenotypic aspects and preliminary molecular mechanisms. Although we have demonstrated the superior promoting effect of 3D microscaffolds loaded with BMSCs on osteoblasts through these investigations, the intricate mechanisms underlying cell-cell interactions have not been elucidated. Future studies will focus on analyzing these molecular mechanisms. Additionally, our *in vivo* experiments were conducted on small rodent models, which may not fully reflect the reparative effects in humans. Subsequent research will be carried out on larger primate models to provide high-quality evidence supporting the clinical application of 3D microscaffolds loaded with low-dose BMSCs for early-stage femoral head osteonecrosis treatment.

5. Conclusion

The treatment of early-stage steroid-induced femoral head osteonecrosis using a single injection of 3D microscaffolds loaded with low-dose BMSCs has achieved therapeutic outcomes similar to those achieved with the injection of high-dose free BMSCs. This clearly demonstrates the advantages of this treatment approach, as it significantly reduces the number of required cells and opens up possibilities for large-scale clinical applications. Additionally, this study represents the first exploration of the therapeutic effects of 3D microscaffolds loaded with BMSCs for early-stage steroid-induced femoral head osteonecrosis, and provides a preliminary investigation into the underlying molecular mechanisms, providing a promising treatment strategy for the hip-preserving therapy of femoral head osteonecrosis.

CRediT authorship contribution statement

Minzheng Guo: Writing – original draft, Supervision, Resources, Methodology, Funding acquisition, Formal analysis, Data curation, Conceptualization. **Baochuang Qi:** Writing – review & editing, Software, Methodology, Investigation, Data curation, Conceptualization. **Zijie Pei:** Validation, Software, Methodology, Investigation. **Haonan Ni:** Software. **Junxiao Ren:** Software. **Huan Luo:** Software, Methodology. **Hongxin Shi:** Validation, Software. **Chen Meng:** Data curation, Validation. **Yang Yu:** Software, Methodology. **Zhifang Tang:** Software. **Yongqing Xu:** Writing – review & editing, Supervision, Resources, Project administration, Investigation, Funding acquisition, Formal analysis, Conceptualization. **Qingyun Xue:** Writing – review & editing, Supervision, Resources, Investigation, Data curation. **Chuan Li:** Writing – review & editing, Supervision, Resources, Project administration, Investigation, Funding acquisition, Data curation, Conceptualization.

Ethics approval and consent to participate

The experimental protocol has been approved by the Ethics Committee of the 920th Hospital of the Chinese People's Liberation Army Joint Logistic Support Force (LS-2022-039(K)-01).

Consent for publication

Not applicable.

Availability of data and materials

A Data Availability statement is not applicable to this manuscript.

Declaration of AI and AI-assisted technologies in the writing process

No AI or AI-assisted technologies were used in the writing or editing of this manuscript.

Funding

This work was jointly supported by the Grants from Yunnan Orthopedics and Sports Rehabilitation Clinical Medicine Research Center Fund (grant numbers 202102AA310068), Yunnan Province Clinical Orthopaedic Trauma Medical Center Fund (grant numbers ZX20191001), Yunnan Province Science and Technology Talents and Platform Program Project Fund (grant numbers 202105AD160027), Meiluo Young Physicians' Innovative Development Project Fund (grant numbers GSKQNJJ-2023-005).

Declaration of competing interest

The authors declare no conflict of interest.

Acknowledgements

Not applicable.

Appendix A. Supplementary data

Supplementary data to this article can be found online at https://doi.org/10.1016/j.mtbio.2024.101426.

Data availability

Data will be made available on request.

References

[1] C. Huang, Z. Wen, J. Niu, et al., Steroid-induced osteonecrosis of the femoral head: novel insight into the roles of bone endothelial cells in pathogenesis and treatment, Front. Cell Dev. Biol. 9 (2021) 777697.
[2] D. Zhao, F. Zhang, B. Wang, et al., Guidelines for clinical diagnosis and treatment of osteonecrosis of the femoral head in adults (2019 version), J Orthop Translat 21 (2020) 100–110.
[3] Y. Chen, Y. Miao, K. Liu, et al., Evolutionary course of the femoral head osteonecrosis: histopathological - radiologic characteristics and clinical staging systems, J Orthop Translat 32 (2022) 28–40.
[4] M. Chughtai, N.S. Piuzzi, A. Khlopas, et al., An evidence-based guide to the treatment of osteonecrosis of the femoral head, Bone Joint Lett. J 99-b (10) (2017) 1267–1279.
[5] L. Zhao, A.D. Kaye, A.J. Kaye, et al., Stem cell therapy for osteonecrosis of the femoral head: current trends and comprehensive review, Curr. Pain Headache Rep. 22 (6) (2018) 41.
[6] Z. Wen, Y. Li, Z. Cai, et al., Global trends and current status in osteonecrosis of the femoral head: a bibliometric analysis of publications in the last 30 years, Front. Endocrinol. 13 (2022) 897439.
[7] D. Petek, D. Hannouche, D. Suva, Osteonecrosis of the femoral head: pathophysiology and current concepts of treatment, EFORT Open Rev 4 (3) (2019) 85–97.
[8] B. Atilla, S. Bakircioğlu, A.J. Shope, et al., Joint-preserving procedures for osteonecrosis of the femoral head, EFORT Open Rev 4 (12) (2019) 647–658.
[9] M.A. Mont, H.S. Salem, N.S. Piuzzi, et al., Nontraumatic osteonecrosis of the femoral head: where do we stand today?: a 5-year update, J Bone Joint Surg Am 102 (12) (2020) 1084–1099.
[10] D. Zhao, Z. Ma, Application of biomaterials for the repair and treatment of osteonecrosis of the femoral head, Regen Biomater 7 (1) (2020) 1–8.
[11] Y. Xu, Y. Jiang, C. Xia, et al., Stem cell therapy for osteonecrosis of femoral head: opportunities and challenges, Regen Ther 15 (2020) 295–304.
[12] H. Xu, C. Wang, C. Liu, et al., Cotransplantation of mesenchymal stem cells and endothelial progenitor cells for treating steroid-induced osteonecrosis of the femoral head, Stem Cells Transl Med 10 (5) (2021) 781–796.
[13] N. Yang, H. Sun, Y. Xue, et al., Inhibition of MAGL activates the Keap1/Nrf2 pathway to attenuate glucocorticoid-induced osteonecrosis of the femoral head, Clin. Transl. Med. 11 (6) (2021) e447.
[14] D. Xing, W. Liu, B. Wang, et al., Intra-articular injection of cell-laden 3D microcryogels empower low-dose cell therapy for osteoarthritis in a rat model, Cell Transplant. 29 (2020) 963689720932142.
[15] Z.Y. Wu, Q. Sun, M. Liu, et al., Correlation between the efficacy of stem cell therapy for osteonecrosis of the femoral head and cell viability, BMC Muscoskel. Disord. 21 (1) (2020) 55.
[16] B. Wang, W. Liu, J.J. Li, et al., A low dose cell therapy system for treating osteoarthritis: in vivo study and in vitro mechanistic investigations, Bioact. Mater. 7 (2022) 478–490.
[17] R. Li, Q.X. Lin, X.Z. Liang, et al., Stem cell therapy for treating osteonecrosis of the femoral head: from clinical applications to related basic research, Stem Cell Res. Ther. 9 (1) (2018) 291.
[18] W. Zhou, M. Qu, Y. Lv, et al., New advances in stem cell therapy for osteonecrosis of the femoral head, Curr. Stem Cell Res. Ther. 14 (3) (2019) 226–229.
[19] B. Liu, F. Yang, X. Wei, et al., An exploratory study of articular cartilage and subchondral bone reconstruction with bone marrow mesenchymal stem cells combined with porous tantalum/Bio-Gide collagen membrane in osteonecrosis of the femoral head, Mater Sci Eng C Mater Biol Appl 99 (2019) 1123–1132.
[20] B. Li, Y. Lei, Q. Hu, et al., Porous copper- and lithium-doped nano-hydroxyapatite composite scaffold promotes angiogenesis and bone regeneration in the repair of glucocorticoids-induced osteonecrosis of the femoral head, Biomed. Mater. 16 (6) (2021).
[21] S. Murab, T. Hawk, A. Snyder, et al., Tissue engineering strategies for treating avascular necrosis of the femoral head, Bioengineering (Basel) 8 (12) (2021).
[22] Z. Fu, Y. Lai, Y. Zhuang, et al., Injectable heat-sensitive nanocomposite hydrogel for regulating gene expression in the treatment of alcohol-induced osteonecrosis of the femoral head, APL Bioeng. 7 (1) (2023) 016107.
[23] D. Xing, W. Liu, J.J. Li, et al., Engineering 3D functional tissue constructs using self-assembling cell-laden microniches, Acta Biomater. 114 (2020) 170–182.
[24] X. Yan, K. Zhang, Y. Yang, et al., Dispersible and dissolvable porous microscaffold tablets enable efficient large-scale human mesenchymal stem cell expansion, Tissue Eng. C Methods 26 (5) (2020) 263–275.
[25] H. Yu, Z. You, X. Yan, et al., TGase-enhanced microtissue assembly in 3D-printed-template-scaffold (3D-MAPS) for large tissue defect reparation, Adv. Healthcare Mater. 9 (18) (2020) e2000531.
[26] D.T. Chu, T.N.T. Phuong, N.L.B. Tien, et al., An update on the progress of isolation, culture, storage, and clinical application of human bone marrow mesenchymal stem/stromal cells, Int. J. Mol. Sci. 21 (3) (2020).
[27] J. Dang, J. Yang, Z. Yu, et al., Bone marrow mesenchymal stem cells enhance angiogenesis and promote fat retention in fat grafting via polarized macrophages, Stem Cell Res. Ther. 13 (1) (2022) 52.
[28] W. Liu, Y. Li, S. Feng, et al., Magnetically controllable 3D microtissues based on magnetic microcryogels, Lab Chip 14 (15) (2014) 2614–2625.
[29] L. Wang, B.L. Heckmann, X. Yang, et al., Osteoblast autophagy in glucocorticoid-induced osteoporosis, J. Cell. Physiol. 234 (4) (2019) 3207–3215.
[30] N. Maruotti, A. Corrado, F.P. Cantatore, Osteoblast role in osteoarthritis pathogenesis, J. Cell. Physiol. 232 (11) (2017) 2957–2963.
[31] L. Shen, G. Hu, C.M. Karner, Bioenergetic metabolism in osteoblast differentiation, Curr. Osteoporos. Rep. 20 (1) (2022) 53–64.
[32] C. Qiu, Study on Preventing Glucocorticoid-Induced Osteonecrosis of Femoral Head in Human Umbilical Cord Mesenchymal Stem Cells [D], Wuhan University, 2021.
[33] J. Xu, H. Gong, S. Lu, et al., Animal models of steroid-induced osteonecrosis of the femoral head-a comprehensive research review up to 2018, Int. Orthop. 42 (7) (2018) 1729–1737.
[34] C. Chang, A. Greenspan, M.E. Gershwin, The pathogenesis, diagnosis and clinical manifestations of steroid-induced osteonecrosis, J. Autoimmun. 110 (2020) 102460.
[35] S. Yamanaka, Pluripotent stem cell-based cell therapy-promise and challenges, Cell Stem Cell 27 (4) (2020) 523–531.
[36] X. Cao, L. Duan, H. Hou, et al., IGF-1C hydrogel improves the therapeutic effects of MSCs on colitis in mice through PGE(2)-mediated M2 macrophage polarization, Theranostics 10 (17) (2020) 7697–7709.
[37] J. Jin, Stem cell treatments, JAMA 317 (3) (2017) 330.
[38] W. Zakrzewski, M. Dobrzyński, M. Szymonowicz, et al., Stem cells: past, present, and future, Stem Cell Res. Ther. 10 (1) (2019) 68.
[39] S. Lopa, A. Colombini, M. Moretti, et al., Injective mesenchymal stem cell-based treatments for knee osteoarthritis: from mechanisms of action to current clinical evidences, Knee Surg. Sports Traumatol. Arthrosc. 27 (6) (2019) 2003–2020.
[40] C. Zhang, B. Xie, Y. Zou, et al., Zero-dimensional, one-dimensional, two-dimensional and three-dimensional biomaterials for cell fate regulation, Adv. Drug Deliv. Rev. 132 (2018) 33–56.
[41] P.W. Zandstra, A. Nagy, Stem cell bioengineering, Annu. Rev. Biomed. Eng. 3 (2001) 275–305.
[42] T.C. Johnson, D. Siegel, Directing stem cell fate: the synthetic natural product connection, Chem. Rev. 117 (18) (2017) 12052–12086.
[43] N.E. Ryu, S.H. Lee, H. Park, Spheroid culture system methods and applications for mesenchymal stem cells, Cells 8 (12) (2019).
[44] F. Zhang, W. Peng, T. Wang, et al., Lnc Tmem235 promotes repair of early steroid-induced osteonecrosis of the femoral head by inhibiting hypoxia-induced apoptosis of BMSCs, Exp. Mol. Med. 54 (11) (2022) 1991–2006.
[45] D.T. Scadden, The stem-cell niche as an entity of action, Nature 441 (7097) (2006) 1075–1079.
[46] S.R. Singh, Stem cell niche in tissue homeostasis, aging and cancer, Curr. Med. Chem. 19 (35) (2012) 5965–5974.